Published in final edited form as:
Nat Cell Biol. 2015 March ; 17(3): 340–349. doi:10.1038/ncb3104.

A high throughput platform for stem cell-niche co-cultures and downstream gene expression analysis

Adam D Gracz[1,2], **Ian A Williamson**[2], **Kyle C Roche**[1], **Michael J Johnston**[2], **Fengchao Wang**[6,7], **Yuli Wang**[3], **Peter J Attayek**[4], **Joseph Balowski**[3], **Xiao Fu Liu**[2], **Ryan J Laurenza**[2], **Liam T Gaynor**[2], **Christopher E Sims**[3], **Joseph A Galanko**[2], **Linheng Li**[5,6], **Nancy L Allbritton**[3,4], and **Scott T Magness**[1,2,4]

[1]University of North Carolina at Chapel Hill Dept of Cell Biology & Physiology, Chapel Hill, North Carolina 27599

[2]University of North Carolina at Chapel Hill Dept of Medicine, Chapel Hill, North Carolina 27599

[3]niversity of North Carolina at Chapel Hill Dept of Chemistry, Chapel Hill, North Carolina 27599

[4]UNC/NC State Biomedical Engineering, Chapel Hill, North Carolina 27599

[5]Stowers Institute for Medical Research, Kansas City, Missouri 64110

[6]University of Kansas, Dept of Pathology and Laboratory Medicine, Kansas City, Kansas 66160

Abstract

Stem cells reside in “niches”, where support cells provide signaling critical for tissue renewal. Culture methods mimic niche conditions and support the growth of stem cells *in vitro*. However, current functional assays preclude statistically meaningful studies of clonal stem cells, stem cell-niche interactions, and genetic analysis of single cells and their organoid progeny. Here, we describe a “microraft array” (MRA) that facilitates high-throughput clonogenic culture and computational identification of single intestinal stem cells (ISCs) and niche cells co-cultures. We use MRAs to demonstrate that Paneth cells, a known ISC niche component, enhance organoid formation in a contact-dependent manner. MRAs facilitate retrieval of early enteroids for qPCR to correlate functional properties, such as enteroid morphology, with differences in gene expression. MRAs have broad applicability to assaying stem cell-niche interactions and organoid development, and serve as a high-throughput culture platform to interrogate gene expression at early stages of stem cell fate choices.

Correspondence should be addressed to: Scott T. Magness, University of North Carolina at Chapel Hill, 111 Mason Farm Rd. CB# 7032, MBRB Rm. 4337, Chapel Hill, North Carolina 27599, Tel: 919-966-6816, Fax: 919-843-6899, magness@med.unc.edu.
[7]present address: Third Military Medical University, College of Preventative Medicine, Institute of Combined Injury of PLA, State Key Laboratory of Trauma, Burns, and Combined Injury, Chongqing, China 400038

Contributions: A.D.G. and S.T.M. conceived and designed experiments. I.A.W. developed and optimized image analysis algorithms and analyzed data with M.J.J., X.F.L., R.J.L., and L.T.G. Y.W., P.J.A., and J.B microfabricated MRAs. Y.W., C.E.S., and N.L.A. supervised microfabrication and troubleshooting of MRA development. K.C.R. analyzed single cell and enteroid gene expression data. P.J.A. conducted and interpreted COMSOL modeling with N.L.A. F.W. and L.L. developed and provided methodology for highly efficient enteroid culture. J.A.G. conducted statistical analysis of enteroid formation assays. A.D.G. and S.T.M. wrote the manuscript with critical insight and commentary from all co-authors. S.T.M. initiated and supervised the project.

Competing financial interests: N.L.A., C.E.S., Y.W., and S.T.M. disclose a financial interest in Cell Microsystems.

Keywords

stem cell niches; high-throughput assay; intestinal stem cells

Introduction

Understanding how somatic stem cells self-renew and differentiate to produce the functional cells of their resident tissue is essential for determining the mechanisms underlying a broad range of issues related to human health and disease. The intestinal epithelium undergoes one of the most rapid rates of renewal of any mammalian tissue, making it an excellent model system for understanding stem cell driven physiological renewal. While *in vivo* lineage tracing remains an important technique for the analysis of stem cell behavior, developments in primary stem cell culture have expanded the stem cell biologist's toolkit to include powerful, complementary *in vitro* assays [1].

Lgr5^{high} or *Sox9*^{low} ISCs are capable of forming "enteroid" structures *in vitro*, demonstrating multipotency and self-renewal [2-4]. *In vivo*, ISCs are closely associated with Paneth cells (PCs), which function as niche cells and express soluble and insoluble factors associated with stemness, such as Wnt and Notch ligands [5, 6]. PCs have been shown to increase the efficiency of enteroid formation by ISCs *in vitro* [6]. However, these studies relied on the co-culture of hundreds of ISCs with hundreds of PCs, and may not reflect physiological normal conditions in single intestinal crypts, where much smaller numbers of ISCs (∼15) and PCs (∼8) interact [6-8].

Technical limitations hinder efficient functional *in vitro* studies of ISC-niche interactions. Additionally, the field currently lacks a robust assay to study ISCs at the clonal level, a tool that has driven the understanding of stem cell niches in the hematopoietic system and mammary glands [9, 10]. Array-based technologies are emerging as a powerful method to study the functional characteristics of single and/or small numbers of stem cells in the hematopoietic system, and hold similar promise for epithelial tissues such as the intestine [11]. In the present study, we describe a platform to study large numbers of single ISCs simultaneously, either at the clonal level or in the presence of niche cells. Microfabricated culture arrays modified for long-term 3-dimensional culture are used to capture and functionally assay clonal ISCs and ISC-niche cell co-cultures, effectively providing a platform for high-throughput niche reconstruction using primary stem and niche cells. Finally, the platform allows for efficient retrieval of single ISCs and developed enteroids for downstream gene expression analysis at different time points.

Results

Microraft arrays are adaptable to cell culture and imaging

We hypothesized that previously described polydimethylsiloxane (PDMS)/polystyrene "microraft arrays" (MRAs) could be utilized to isolate and culture single ISCs in three-dimensional ECM (Fig. 1A-C) [12]. Since ISCs require several days to develop into enteroids, MRAs had to be amenable to media changes [3, 4]. To meet these requirements, polycarbonate

cassettes, with dividers to create multiple media reservoirs, were bonded to MRAs (Fig. 1A,B, Supplementary Fig. 1H). Cassettes were fabricated with two or four culture chambers (~2,500 or 5,000 microwells per culture chamber, respectively, Fig. 1B). Physical well addresses, stamped into PDMS at 5 microwell intervals, were included in the array design to allow for tracking of single cells and enteroids across many time points (Fig. 1C). Tile-scanning microscopy produced high-resolution images of whole MRAs for downstream analysis (Fig. 1F,I, Supplementary Fig. 2).

Microraft arrays support long-term, clonal intestinal stem cell culture

To facilitate tracking of isolated cells in MRAs, *Sox9*^{EGFP} mice were crossed to *CAG*^{DsRed} mice, which express the *DsRed* fluorescent transgene ubiquitously across all cell and tissue types (Fig. 1D) [3, 13]. *Sox9EGFP*^{low}:*DsRed*+ ISCs were plated in a single culture chamber of a two-chamber MRA, randomly seeded into microwells by centrifugation, and overlaid with Matrigel and ISC-supporting growth factors (Fig. 1E) [6, 14]. This resulted in a random distribution of ISCs across MRAs, with microwells containing one, multiple, or no ISCs (Fig 1F-H). For biocompatibility experiments, we utilized high efficiency ISC culture methods that drive high Wnt and Notch signaling [14]. Tile scanning of the MRA in the *dsRed* wavelength immediately after plating and at 48hrs revealed that isolated ISCs had begun to produce primitive enteroids, indicative of biocompatibility (Fig. 1F-K).

Conventional ISC cultures are capable of supporting enteroid growth for many weeks [4]. ISCs were maintained up to 8 weeks in MRAs, with retention of enteroids in their original microwells (Fig. 1L,M). At 8 weeks, enteroids had grown into large structures containing many crypts (Fig. 1M). These observations demonstrate feasibility for long-term MRA-based culture of primary ISCs.

Post-hoc image analysis identifies microwells containing a single stem cell

To rapidly assess the cellular contents in each of the microwells, we developed a computational pipeline with the following analytical goals: 1) to identify microwells containing ISCs, 2) exclude empty microwells, 3) exclude microwells containing debris or imaging artifacts, and 4) quantify the number of ISCs per microwell (Fig. 2A). To achieve this, we developed an image analysis computational pipeline (Fig. 2; Supplementary Methods) [15].

Computational analysis was able to accurately identify microwells containing the targeted number of initial cells, especially for single ISCs (99.87%; n=2258 visually validated) (Fig. 2H). Due to stringency settings adapted specifically for clonal analysis, the percent of identified microwells was reduced for wells containing multiple cells, but the incidence of falsely identified microwells remained 0% for all cell numbers examined (Fig. 2H,I).

Sox9^{EGFP} transgenic mice facilitate high-purity isolation of Paneth cells

To provide proof-of-concept for stem cell niche experiments using MRAs, we sought to co-culture ISCs and PCs to assess clonal and PC-influenced enteroid formation *in vitro*. Previous studies have isolated PCs by FACS of CD24^{High}:SSC^{High} populations [6]. However, CD24 is also expressed on ISCs, TAs, and enteroendocrine cells [3, 14, 16-18]. Since the

experimental approach of MRA cultures examines events on a “per well” basis, it was critical to refine isolation procedures for PCs to meet purity requirements of clonal and microscale co-cultures and avoid artifactual results due to contaminating non-PC cell types. Previous characterization of the *Sox9*^{EGFP} mouse model demonstrated that *Sox9* is expressed at different levels in ISCs, progenitors, and enteroendocrine cells, but that the *Sox9*^{EGFP} transgene is preferentially silenced in PCs [7]. We exploited this property to isolate a highly pure population of PCs by FACS exclusion of *Sox9*^{EGFP} populations. PCs were FACS-isolated using CD24^{High}:SSC^{High} parameters, and the additional exclusion of all *Sox9*^{EGFP}-positive cells (Supplementary Fig. 3B,C). Gene expression analysis revealed a 2-fold increase in lysozyme expression, a 5-fold decrease in *Lgr5* expression, and a >10-fold decrease in *Chga* using *Sox9*^{EGFP} exclusion, indicating de-enrichment of ISCs and enteroendocrine cells (Supplementary Fig. 4).

PC purity was further examined by single cell qPCR on 96 *Sox9*^{EGFP}-excluded PCs. *Sox9EGFP*^{neg}:CD24^{High}:SSC^{High} cells were morphologically consistent with PCs, exhibiting typical granulation and large cell size (Fig. 3A). Importantly, all isolated cells expressed the PC-related gene *Defcr-rs* (Fig. 3B,C). *Lgr5* was detected in some cells, consistent with recent reports on *Lgr5* expression in a subset of PCs *in vivo* (Fig. 3C) [19]. Similarly, while all cells were negative for the enteroendocrine transcript *Tac1*, expression of *Chga* was observed in a single PC, consistent with reports of PC progenitors expressing this enteroendocrine marker (Fig. 3C) [19].

Emerging evidence demonstrates that multiple intestinal progenitor cell populations are capable of dedifferentiating and functioning as ISCs *in vitro* and *in vivo* [19-21]. To address the possibility that enteroids might form from early progenitors in the PC population, 2,810 individual PCs were examined in subsequent *in vitro* experiments. We only once observed enteroid production by a cell isolated using *Sox9EGFP*^{neg}:CD24^{High}:SSC^{High} parameters (0.04%). Together, these data indicate that *Sox9EGFP*^{neg}:CD24^{High}:SSC^{High} populations are genotypically and phenotypically consistent with mature PCs.

Paneth cell-ISC contact is required for increased enteroid formation *in vitro*

As previous studies have speculated that PC-secreted WNTs are responsible for enhancing ISC growth *in vitro*, ISC-PC co-culture experiments were carried out in the absence of exogenous WNT, to avoid “masking” the potential impact of PCs on enteroid formation [4-6]. The GSK3β-inhibitor CHIR99021, a WNT agonist, was also excluded from co-culture experiments. To address the possibility that a PC in one microwell might affect the growth of an ISC in an adjacent, but separate microwell, we modeled diffusion dynamics of cell secreted molecules in MRAs. Diffusion between microwells was deemed negligible under models relying on liberal rates of diffusion and decay (Supplementary Note 1).

We hypothesized that increased numbers of PCs would result in increased Wnt secretion and ISC growth, and examined microwells with initial contents consisting of any combination of 1-5 ISCs and 0-2 PCs. ISCs were isolated from *Sox9*^{EGFP} or *Lgr5*^{EGFP} mice and PCs from *Sox9*^{EGFP}:*CAG*^{DsRed} mice (Fig. 4A). *DsRed* fluorescence was used as a readout of ISC contamination in PC populations. Replicate experiments were conducted for each ISC biomarker to increase sample size per ISC-PC combination, and data were analyzed from

four total MRA experiments, consisting of 4,830 data points, each corresponding to an individual microwell containing any combination of ISCs and PCs (Supplementary Table 1). Surprisingly, examination of survival percentages across all combinations of ISCs and PCs revealed no statistically significant trends, regardless of whether ISCs were isolated using *Sox9*^{EGFP} or *Lgr5*^{EGFP} (Fig. 4B,C). To investigate the overall effect of PCs on enteroid survival, we next analyzed the percentage of enteroids formed in microwells containing any number of ISCs or any number of ISCs with any number of PCs (Fig. 4D). These analyses also failed to produce statistically significant differences between ISC-only and ISC-PC microwells, suggesting that PC presence alone is insufficient to increase enteroid formation *in vitro* at physiologically relevant numbers.

Previous studies have suggested that cell-to-cell contact between ISCs and PCs may influence enteroid formation, but this has not been formally tested by comparison between touching and non-touching ISCs and PCs [6]. Using the same data generated in our ISC-PC co-culture experiments, we reanalyzed initial MRA contents to classify microwells by cell-to-cell contacts at t=0hr and correlated this status with enteroid formation outcome (Fig. 4E). This comparison yielded results with overall statistical significance (conditional logistic regression, $p = 0.0282$), indicating that ISCs in direct contact with PCs are more likely to form enteroids than ISCs alone, or ISC-PC wells that are not in direct contact. Interestingly, ISC-ISC contact events were also more likely to form enteroids than non-touching ISCs, suggesting that cell-to-cell contact between two or more ISCs may also positively influence enteroid formation. As expected, PC-PC contact did not result in the formation of enteroids, consistent with the post-mitotic status of PCs *in vivo* and the high level of purity observed in PC populations (Fig. 4G).

Single cells do not form *de novo* contacts after plating

The contact-dependent effects on enteroid formation prompted us to ask if *de novo* cell-cell contacts occurred after initial classification as “non-touching” at t=0hr. To assay this, we measured the distance between ISC-ISC, ISC-PC, and PC-PC pairs in microwell images acquired at t=0hr and calculated positive or negative changes in cell-cell distance at t=24hr (Fig. 5). Microwells in which both cells were alive at 24hr were included for analysis, resulting in $n = 905$ pairs (521 ISC-ISC; 345 ISC-PC; 39 PC-PC) (Fig. 5B). To control for background movement due to known changes in extracellular matrix integrity that occur over time, measurements were taken on pairs of fixed intestinal epithelial cells for comparison ($n = 50$). Analysis of change in distance in alive pairs demonstrated that: 1) cell movement was statistically significant compared to measurements taken on pairs of fixed cells, and 2) no observed cells formed *de novo* contacts after initial plating of MRAs. Interestingly, non-touching pairs of cells with an initial cell-cell distance ≤ 25μm appear to grow further apart within the first 24hrs of culture (Fig. 5C). Together, these data demonstrate that single cells migrate within Matrigel cultures and that cell-cell signaling may repel single cells from one another over short distances *in vitro*.

Previous studies demonstrate significant enteroid movement and merger *in vitro* [6]. To further examine cell movement in the MRA platform, we performed time-lapse imaging of microwells. Single cells demonstrated appreciable movement as they developed into

enteroids over the first 24hrs of culture (Supplementary Movie 1). Larger clumps of cells merged into single enteroids, suggesting that the movement and merger of ISCs *in vitro* may be influenced by cell number or heterogeneity within populations (Supplementary Movie 2).

Modified MRAs facilitate genetic analysis of enteroid development

Microscale culture systems for primary tissues are potentially powerful tools for high-throughput screening, drug discovery, and personalized medicine. The power of such platforms is enhanced when differences in phenotype, such as organoid size or morphology, can be correlated with differences in gene expression. We reasoned that MRAs could be utilized to examine genetic heterogeneity in single ISCs, early enteroids (2-3 cell), and developed enteroids. To facilitate single ISC and enteroid retrieval for downstream analysis, MRAs were modified so that standard polystyrene rafts at the bottom of each microwell were replaced with magnetized rafts, as recently described (Supplementary Fig. 5A) [12, 22]. A raft release device was fitted to a 10X objective to liberate the rafts from the PDMS wells, and a magnetic wand was used to retrieve rafts for transfer to RNA lysis buffer (Supplementary Fig. 5A-D). Rafts containing single *Lgr5*^{high} ISCs or enteroids were retrieved and cDNA was generated from a total of 192 rafts, representing single ISCs, early enteroids, and developed enteroids, across 6 times points (Fig. 6A and Supplementary Fig. 5G). High-throughput qPCR was then used to assess the expression of 20 genes associated with ISCs, progenitors, and post-mitotic lineages (Fig. 6B&C). Representative analysis of *Sox9*, *Hopx*, and *Ccnd1* in empty rafts (n=12) produced a only a single Ct value for *Sox9* (Ct = 36.97 of 40 cycles), but did not produce a visible band by gel electrophoresis, demonstrating negligible background in retrieved rafts.

As expected, *Lgr5* mRNA was highly expressed by single ISCs, demonstrating population purity (Fig. 6C). Though other crypt-base columnar ISC markers *Olfm4* and *Smoc2* were strongly detected in single ISCs, a number of cells were negative for putative "+4" ISC markers *Bmi1*, *Hopx*, and *Tert*, contrary to studies conducted on populations of *Lgr5*^{high} cells [23-26]. To test if this finding was reflective of a transcriptional response to ISC culture conditions, we compared gene expression profiles of single *Lgr5*^{high} cells sorted directly into lysis buffer with those exposed to Matrigel culture with and without growth factors/ small molecules (EGF, Noggin, Jagged-1, CHIR99021, LY2157299, and Thiazovivin). While growth factors specifically elicited upregulation of *Lgr5*, *Olfm4*, and *Lyz2* in single cells, *Lgr5*^{high} ISCs exhibited heterogeneity in terms of *Bmi1*, *Hopx*, and *Tert* regardless of exposure to culture conditions (Fig. 7). Together, these data demonstrate that ISC culture conditions upregulate ISC-associated genes and *Lyz2* in single cells and suggest transcriptional heterogeneity for *Bmi1*, *Hopx*, and *Tert* in *Lgr5*^{high} cells.

Gene expression changes in developing enteroids were consistent with cellular differentiation (Fig. 6C). *Hes1* was enriched at 24hrs post-plating, suggesting initiation of Notch signaling, which was recently shown to be important for progenitor fate decisions [27]. Subsequently, *Dll1* expression initiates in a majority of enteroids at 48-hours, consistent with the emergence of secretory progenitor populations [21, 28]. Early expression of *Sis* appears to be coincident with upregulation *Hes1*, a known driver of enterocyte fate, while *Muc2* and *Chga* are upregulated at later time points, coincident with increased *Atoh1*

expression [29, 30]. By 10 days in culture, enteroids are enriched for the expression of transcripts associated with absorptive enterocytes (*Sis*), goblet cells (*Muc2*), PCs (*Lyz, Defr-rs1*), and endocrine cells (*Chga*, *Chgb*), consistent with a fully developed organoid phenotype (Fig. 6B,C) [4].

MRAs reveal genetic differences associated with enteroid phenotype

While enteroid development demonstrated an expected pattern of gene expression associated with differentiation, we noted bimodal distribution of several genes across the developmental timeline, suggesting heterogeneity in enteroid populations (Fig. 6C). To examine this, we chose two previously observed morphologies, cystic and columnar, and collected enteroids for gene expression analysis at 24hr and 48hr, based on these morphologies (Fig. 6D) [5]. The cellular “monolayer” of cystic enteroids was determined to be significantly thinner than that of columnar enteroids, confirming the morphological difference (Fig. 6E). Since cystic enteroid morphology is observed coincident with increased Wnt signaling, we expanded our analysis to include genes associated with Wnt and cell cycle (Supplementary Fig. 6 and 7) [5]. Principle components analysis revealed that enteroids were similar at 24hr, regardless of morphology (Fig. 6F). However, at 48hr, cystic enteroids exhibited dissimilar gene expression profiles relative to columnar enteroids at the same time point. Most notably, genes associated with cell cycle progression, *Ccnb1*, *Ccnd1*, and *Ccne1* were upregulated in cystic enteroids relative to columnar enteroids at 48hr (Fig. 6G). Additionally, more cystic enteroids exhibited higher expression levels of ISC markers *Lgr5* and *Ascl2*, and Wnt receptor *Fzd6* at 48hr, compared to columnar enteroids. Together, these data suggest that cystic morphology in early enteroids correlates with a proliferative phenotype, and demonstrate the ability to dissect functional and phenotypic changes at the genetic level using the MRA platform.

Discussion

Stem cell niches provide critical extrinsic signals that govern stem cell self-renewal and differentiation, but their anatomical locations and complexity often present significant challenges to the study of stem cell-niche interactions *in vivo*. As an alternative approach, *in vitro* techniques that rely on the co-culture of isolated stem and niche cell populations have recently been used to assess the impact of individual niche components on stem cell behavior [6, 31]. However, these methods commonly rely on large numbers of cells, which may not reflect physiologically relevant niche behavior, and are not amenable to high-throughput studies. Here, we present an array-based platform that facilitates the study of thousands of isolated stem and niche cells.

PCs express soluble and insoluble ISC niche signaling components, including Wnt and Notch ligands [5, 6]. In the present study, we examine the impact of PC presence and contact with ISCs on enteroid formation. Interestingly, we find that PC presence alone is not predictive of enteroid formation. Rather, direct cell-to-cell contact between ISCs and PCs is required for enhanced ISC growth, suggesting that insoluble or very short-range soluble signals support ISCs *in vitro*. These results support *in vivo* findings that stemness is most strongly correlated cells that exist in intimate contact with PCs, and provide insight to the

functional role of PCs in maintaining stemness [6]. Importantly, the MRA platform was critical in testing dose and contact-dependency of PCs in a microscale format.

In addition to providing a robust platform for studying functional outcomes of clonal stem cells or stem cell-niche cultures, MRAs allow for the retrieval of single cells and organoids for downstream analysis. This ability enhances the power of MRAs by integrating high-throughput functional and genetic/genomic data. We used magnetic MRAs in combination with microfluidic qPCR technologies to assess gene expression in single cells and small populations, such as 2-3 cell enteroids. This allowed for observations of gene expression changes over the course of enteroid development, as well as proof-of-principle analysis of morphological differences in early enteroids. These data experimentally reinforce a previously observed correlation between cystic enteroid morphology and increased Wnt signaling, by demonstrating that cystic enteroids express higher levels of genes associated with stemness and active proliferation [5]. Together with methodology for low-input RNA-seq, MRAs potentiate screening of genetic mutants and drugs/small molecules at the genomic level [32].

Array-based stem cell culture platforms are growing in use and present an efficient and cost-effective alternative to conventional cell culture [33, 34]. However, most platforms are not amenable to long-term cultures, such as required for the development of ISC-derived enteroids and other self-assembled, stem cell derived organoids [35-38]. MRAs facilitate the culture of thousands of primary stem cells over many days and weeks as well as high throughput reconstitution of the stem cell niche at physiologically relevant cell numbers. The power of the MRA platform is further highlighted by the ability to retrospectively “mine” existing high-throughput MRA datasets to test new hypotheses, such as niche cell dose-dependency, cell-cell contact, and cellular movement within microwells.

MRAs provide robust methodology for screening candidate mitogens and morphogens for their effect on enteroid formation and development, and the study of other ISC niche cells, such as pericryptal myofibroblasts, endothelial cells, and neurons. Additionally, MRAs have broad potential for *in vitro* reconstruction of stem cell niches across a range of cell and tissue types, especially those that require three-dimensional ECM. The ability to easily retrieve a high replicate number of organoids early in their development allows investigators to associate functional observations with dynamic changes at the genetic and transcriptomic level, facilitating next-generation forward genetic screens in primary stem cells.

Experimental Procedures

Mice/phenotyping

Sox9^{EGFP} transgenic mice were originally generated by the GENSAT Brain Atlas Project, and are maintained on an outbred CD-1 background [39]. *Lgr5*$^{EGFP\text{-}CreERT2}$ mice were obtained from Jackson Labs (stock number: 008875, Jackson Laboratory, Bar Harbor, ME) [40]. Male and female mice were used. For microwell array experiments requiring constitutive expression of *dsRed* in isolated ISCs, heterozygous *Sox9*^{EGFP} mice were bred to homozygous *CAG*^{dsRed} mice to produce *Sox9*^{EGFP}:*CAG*^{dsRed} offspring heterozygous for both alleles. *Sox9*^{EGFP}:*CAG*^{dsRed} were phenotyped by examining tail snips taken at ∼10

days postnatal for EGFP and DSRED fluorescence by epifluorescent microscopy. *Lgr5*$^{EGFP\text{-}CreERT2}$ mice were genotyped by previously described PCR protocols [40]. All experiments were conducted on adult mice between 8 and 16 weeks of age. All protocols for animal use were reviewed and approved by the University of North Carolina Institutional Animal Care and Use Committee.

Plating ISCs in microraft arrays

Isolated ISCs and Paneth cells were plated in microraft arrays (Cell Microsystems, Chapel Hill, NC) at ratios of ~1.5 cells: 1 microwell for ISCs and ~1 cell: 2 microwells for Paneth cells. Sorted cells were added to array reservoirs in ISC Sort/Culture Media and cells were seeded into microwells by centrifugation at 51g for 5min at 4°C (Fig. 1E). Following centrifugation, media was gently aspirated and arrays were overlaid with 600uL (2 reservoir array) or 200uL (4 reservoir array) Matrigel and growth factors. Arrays were centrifuged a second time at 51g for 5min at 4°C, to recapture any cells displaced by the addition of Matrigel. Matrigel was allowed to polymerize for 30min at 37°C before being overlaid with 1mL (2 reservoir array) or 600uL (4 reservoir array) ISC Sort/Culture Media. Matrigel for validation experiments contained previously described growth factors, with some modification, at the time of plating: 15μM JAGGED-1 peptide (AnaSpec, San Jose, CA), 750ng/mL EGF (R&D, Minneapolis, MN), 100ng/mL NOGGIN (Peprotech, Rocky Hill, NJ), and 500nM LY2157299 (Selleck Chemicals) [41]. Initial media in validation experiments contained 2.5μM CHIR99021 (Selleck Chemicals) and 2.5μM Thiazovivin (Selleck Chemicals). Growth factors were added at two day intervals: 1μM JAGGED-1 peptide, 50ng/mL EGF, 100ng/mL NOGGIN, and 1μg/mL R-SPONDIN1 (R&D). Media was changed every four days, and no CHIR99021 or Thiazovivin was used past initial plating. For ISC/PC co-culture experiments, the following growth factors were used: 1μM JAGGED-1 peptide, 50ng/mL EGF, 100ng/mL NOGGIN, and 1μg/mL R-SPONDIN1. In ISC/PC co-culture experiments, growth factors, minus JAGGED-1 peptide and Y27632, were supplemented every two days, and media was changed every four days, as previously described [42, 43].

Image acquisition, stitching, and segmenting

Microwell arrays were tile-scanned in brightfield, GFP, and dsRed wavelengths using an automated stage and the Scan Slide function in the Metamorph Imaging Suite (Molecular Devices, Sunnydale, CA) immediately after plating and overlaying media (Fig. S3B). Arrays were housed in a physiological chamber mounted on a fluorescent microscope during imaging, in order to prevent cell death due to the imaging procedure. Scanned images were stitched into a single composite image using the open source image analysis suite FIJI [44] and then segmented into address-associated individual well images using an algorithm, “Segmenter.m”, designed in MATLAB (MathWorks, Natick, MA). CellProfiler based image analysis is described in detail in Supplementary Information. Source files for “Segmenter.m”, CellProfiler 2.0 pipeline “SCPipeline.cp”, and “WellContents.xls” are available here as Supplementary Software and for download at http://www.magnesslab.org/#!vstc1=page-1/vstc0=software-downloads.

Raft retrieval and generation of cDNA from single ISCs and enteroids

FACS-isolated *Lgr5*^{EGFP} ISCs were applied to the MRA device at a density that favored single cell (22,500 *Lgr5*^{high}+ cells for 15,000 wells). 24-36 rafts containing either single *Lgr5*^{EGFP} ISCs, developing enterospheres, or fully developed enteroids were collected at the time points described. Raft retrieval was conducted on an Olympus IX-81 microscope fitted with a physiologic chamber to maintain humidity and temperature. Microwells containing an ISC or enteroid were identified and imaged prior to release of the raft. Rafts were released using the commercially available IsoRaft release and retrieval system (Cell Microsystems, Chapel Hill, NC), consisting of a mechanically actuated needle fitted to a standard objective lens. Following liberation of the raft from the PDMS well, the magnetic microwand (Cell Microsystems, Chapel Hill, NC) was used to collect the raft which was then transferred to a single well of a U-bottomed 96-well plate containing 5 μl of RNA lysis buffer (CellsDirect, Life Technologies, Grand Island, NY). Rafts were retrieved in 44.8 ± 14.3s with a retrieval success rate of 93.3% (n = 30 rafts). When accounting for time spent locating and imaging rafts of interest, up to 36 rafts could be collected in approximately 1 hour. DNA removal and cDNA synthesis was conducted according to manufacturer's protocols with the exception that volumes were scaled down to work with a 5μl lysis buffer volume. Specific target amplification (STA) was conducted according to manufacturer's protocols using Taqman probes (Supplementary Table 2). The STA cDNA was applied to a 192.24 Integrated Fluidic Chip (IFC; Fluidigm; South San Francisco, CA) and assayed for gene expression using the Biomark HD platform (Fluidigm). Ct values were normalized to 18S signal and dCT values were analyzed using Fluidigm Real-time PCR analysis software to generate heat maps and and Singular 2.0 (based on R) to generate violin plots.

Fabrication of glass mounted microwell arrays

Materials—SU-8 photoresist was purchased from MicroChem Corp. (Newton, MA). The Sylgard 184 silicone elastomer kit was purchased from Dow Corning (Midland, MI). γ-Butyrolactone (GBL), octyltrichlorosilane, and propylene glycol monomethyl ether acetate were obtained from Sigma-Aldrich (St Luois, MO). Poly(acrylic acid) (MW ∼5,000) was obtained from PolySciences, Inc. (Warrington, PA). Falcon™ Petri dishes were obtained from BD Biosciences (San Jose, CA). Polycarbonate plates (12 inch × 12 inch × 0.5 inch) were purchased from McMaster-Carr (Los Angeles, CA) and glass slides (75 mm × 50 mm × 1 mm) were purchased from Corning Inc. (Corning, NY).

Fabrication of glass-backed PDMS microwell array—An SU-8 master mold with an array of microposts was fabricated using standard photolithography with 100 μm thick SU-8 as described previously [45]. The SU-8 master was coated by octyltrichlorosilane using vapor deposition to render the surface of the master non-sticky to PDMS [46]. Clean glass slides (75 mm × 50 mm × 1 mm) were spin coated with a 15-μm thick layer of poly(acrylic acid) (PAA) by using 50 wt% solution and a spin speed of 2000 rpm, followed by a 1 hr bake on a 100°C hotplate to remove the water. The slide coated in PAA was treated in a plasma cleaner for 10 min (Harrick Plasma, Ithaca, NY). PDMS prepolymer (10 : 1 mixture of base : curing-agent of Sylgard 184 kit) was spread on the SU-8 master mold and degassed under vacuum to remove trapped air bubbles. To control the thickness of the PDMS mold, 300-μm PDMS spacers were placed on both ends of the master mold. PDMS spacers were

created by spin-coating glass with PDMS prepolymer at 200 rpm for 30 s and cured on a 120°C hotplate for 30 min. The plasma-treated PAA-coated glass slide was then placed on the master mold, flattening the PDMS prepolymer between the master mold and the glass slide (supplemental material, Fig. S1A). The ends of the master-glass slide assembly were secured by paper clips to prevent movement during curing of the PDMS. The PDMS was cured in a 95°C oven for 1 hr (supplemental material, Fig. S1B). The glass-backed PDMS microwell array was then obtained by separating the array from the silanized master mold (supplemental material, Fig. S1C). The resulting microwell array has an array area of 25.4 mm × 25.4 mm, and each microwell has a dimension of 200 μm × 200 μm × 100 μm spaced 30 μm apart. Glass-bound MRAs were reproducibly imaged in a single Z-plane without any noticeable out-of-focus sagging (n = 50) (Supplementary Fig. 2).

Micromolding of microraft arrays by dip coating—A polystyrene solution was prepared by dissolving polystyrene Falcon™ Petri dishes in GBL at 20 wt% concentration. The polystyrene solution was spread onto the PDMS microwell array and degassed under vacuum to remove trapped air bubbles (supplemental material, Fig. S1D). The glass-backed PDMS array was then immersed in the polystyrene solution and withdrawn vertically at a speed of 0.83 mm/min by a stepper motor controlled by a custom controller (supplemental material, Fig. S1E). Due to surface tension difference between PDMS and polystyrene solution, polystyrene solution dewetted from the array, resulted in isolated pockets of polystyrene solution in microwells (supplemental material, Fig. S1F). This phenomenon is called discontinuous dewetting [47]. The array was then placed in a 95°C oven overnight to evaporate the GBL solvent, and pockets of polystyrene solution shrunk into solid polystyrene microrafts with a concave geometry (supplemental material, Fig. S1G).

Attaching the array to the cassettes—The array was attached to a rigid 2-chamber or 4-chamber polycarbonate cassette, which was fabricated by computer numerical control (CNC) machine (supplemental material, Fig. S1H). Prior to attachment, the cassette was cleaned by sonication in a solution of 1 wt% detergent in water for 1 hr, followed by a 1 hr sonication in a 75% ethanol solution. The cassette was rinsed thoroughly in DI water and baked for 15 min in a 95°C oven to remove any remaining solvent. Both the array and the cassette were treated in plasma cleaner for 10 min before being glued together with PDMS (cured in a 95°C oven for 1 hr). The arrays were treated with air plasma for 5 min, sterilized with 75% ethanol, and stored in sterile 1X PBS prior to use.

Epithelial isolation and FACS

Epithelial cells were isolated from whole murine intestines, as previously described, with some modifications [48]. Briefly, intestines were opened longitudinally, rinsed in DPBS (Life Technologies, Grand Island, NY), minced, and incubated in 3mM EDTA (Sigma, St Louis, MO) in DPBS for 45min at 4°C with gentle agitation. Intestinal fragments were transferred to fresh DPBS and shaken by hand for 2 minutes to release epithelium. Remnant submucosa was discarded, epithelium was rinsed twice in DPBS, and then dissociated to single cells by incubation in 0.3U/mL dispase (Life Technologies) in 10mL HBSS (Life Technologies) at 37°C for 8-10 min with shaking every 2 minutes. Single epithelial cells were filtered through 100, 70, and 40μm filters before being resuspended in ISC Sort/Culture Media

[Advanced DMEM/F12 (Life Technologies), N2 (Life Technologies), B27 (Life Technologies), Glutamax (Life Technologies), Penicillin/Streptomycin (Life Technologies), 10mM HEPES (Life Technologies), 10μM Y27632 (Selleck Chemicals, Houston, TX), and 500mM N-acetyl-cysteine (Sigma)]. For Paneth cell isolation, cells were resuspended in ISC Sort/Culture Media with 5% FBS (Gemini Biosciences) and stained with the following antibodies: Brilliant Violet conjugated anti-CD24 (1:100; clone M1/69, Biolegend, San Diego, CA); PerCP-Cy5.5 conjugated anti-CD45 (1:100; clone 30-F11, Biolegend). All cells were stained with Sytox Blue (Life Technologies) or 7-AAD (Biolegend) and Annexin V-APC (Life Technologies) prior to FACS, for live-dead exclusion.

FACS was conducted on a MoFloXDP (Beckman Coulter, Pasadena, CA) and *Sox9*^{EGFP} and *Lgr5*^{EGFP} cells were isolated as previously described [40, 48, 49]. Paneth cells were isolated by high expression of CD24, high side-scatter (SSC), and exclusion of CD45, with or without exclusion of *Sox9*^{EGFP} (supplemental material, Fig. S3A&C). Cells were collected into ISC Sort/Culture Media for array culture and RNaqueous lysis buffer for qPCR analysis (Ambion RNaqueous Micro Kit, Life Technologies).

CellProfiler 2.0 analysis

Computational analysis of initial microwell contents was carried out in CellProfiler 2.0 (Broad Institute, Cambridge, MA) in two steps: (1) Segmented microwell images were loaded in sequence into CellProfiler to determine the contents of each microwell of the array. (2) Raw data generated by CellProfiler was converted into easily interpretable graphs and tables displaying the desired location, survivability, or growth of ISCs within the array culture.

Software—Our analysis pipeline (“SCPipeline.cp”) was assembled using modules in the open source image analysis software package CellProfiler 2.0 (available for free download at http://cellprofiler.org).

Image thresholding and object identification—Autofluorescence and reflections off of microwell walls distort the processed microwell images and can reduce the accuracy of stem cell identification. Raw images loaded into CellProfiler undergo thresholding using the “MoG Global” method, which separates objects from background based on an estimate of the amount of the image occupied by objects. The image occupation of a single cell was estimated from 10 microwell images and the threshold correlation factor was increased to prevent background identification. A Laplacian of Gaussian algorithm, which is best used for objects with increasing pixel intensity towards their center (such as dsRed+ cells), was used to distinguish between single and clumped objects.

Filtering objects based on characteristics—To establish parameters for cell identification and debris discrimination, we randomly selected 500 individual microwell images containing single ISCs and 500 individual microwell images containing debris or fluorescent noise from a two-chamber microwell array containing *Sox9*^{EGFP}low:*dsRed*+ ISCs (Fig. 2C). All analysis was conducted on the dsRed wavelength, since the CAG promoter produced a significantly stronger fluorescent signal than the *Sox9*^{EGFP} BAC

transgene. These images were subjected to general size/shape analysis in the CellProfiler 2.0 module “MeasureObjectSizeShape”, which compiled data on the objects' shape and location characteristics. We focused on three specific parameters to develop an analytical pipeline in CellProfiler to identify ISCs: compactness, form factor, and eccentricity. After applying standard image thresholding, CellProfiler identified objects in each microwell in our panel of 1000 images, and we found that ISCs had a distribution of values that was distinct from debris/noise for each of our parameters of interest (Fig. 2D-F). Thresholds were set using these distribution curves to identify ISCs within total identified objects using the “FilterObjects” CellProfiler module (Fig. 2G). The complete pipeline was named “SCPipeline.cp”. A similar approach was used to establish filtering parameters for Paneth cell identification.

Data reconciliation—Data on identified objects and filtered cells contained in each microwell image was exported using the “ExportToSpreadsheet” CellProfiler module and processed using Microsoft Excel for Mac 2011 (Microsoft, Redmond, WA). The object delineated data exported by CellProfiler is converted to well delineated data using “WellContents.xls”, which displays the initial contents of each microwell, the distribution of ISCs and Paneth cell-containing wells in the array, and the addresses of microwells containing cells with no debris or fluorescent noise. Comparison of pre- and post-filtering microwell contents in “WellContents.xls” allowed us to identify the microwell images containing only intact stem cells and no debris (Fig. 2G).

Validation of SCPipeline.cp accuracy—In order to validate our ISC identification pipeline using unbiased microwell images, we manually scored the contents of 2,254 randomly selected microwells. This panel of images was then subjected to analysis using our newly developed pipeline, which was able to identify initial microwell contents with a high degree of accuracy, especially for microwells containing a single ISC (99.87% accurate) (Fig. 2H). Due to stringency settings, this accuracy was reduced for wells containing multiple cells.

Code availability

All software developed for the MRA platform (“Segmenter.m”, “SCPipeline.cp”, and “WellContents.xls”) is available at http://www.magnesslab.org/#!vstc1=page-1/vstc0=software-downloads. Updated versions will be made available as developed. See Supplementary Note 2 for software guide.

Manual analysis of initial microwell contents

For experiments examining enteroid survival relative to initial cell-to-cell contact, tile scanned images of MRAs in EGFP and DsRed wavelengths were overlaid and manually scored by microwell address. DsRed+ cells (isolated as *Sox9EGFP*^{Neg}:*DsRed*$^{+}$:CD24^{High}:SSC^{High}) were considered “PCs” and EGFP+ cells (isolated as *Lgr5EGFP*^{High} or *Sox9EGFP*^{Low}) were considered “ISCs”. Two or more cells were scored as “in contact” only if their fluorescent signatures were contiguous in the overlaid images. For manual quantification of well contents and enteroid survival, all investigators were blinded to prior well contents and survival outcomes.

Statistical analysis of enteroid formation

For cell number experiments, conditional logistic regression was performed with the number of enteroids alive at t = 120hr as the response and the number of ISCs and PCs present in initial well contents as predictors. This was done separately for each experiment as well as separately for each replicate within separate experiments. When analysis was conducted across both replicates in a single experiment, a term indicating individual wells was included in the model to account for well-to-well variability. To examine whether ISC survival was related to cell contact or cell type (ISC or PC) we performed a logistic regression with enteroid survival at t = 120hr as the response and each combination of cell contact and cell type (ISC, no contact; ISC-PC, no contact; ISC-ISC contact; ISC-PC contact) as the predictor. An overall test was performed to examine whether there was any difference in survival amongst the four groups. If overall significance was found then pair wise tests were also performed. Wells were considered independent and therefore it was not necessary to model the correlation between them. No statistical method was used to predetermine sample size and experiments were non-randomized. All analyses were performed using SAS Version 9.3 (SAS Institute Cary NC). P-values less than 0.05 were considered statistically significant.

Quantification of cell movement in microwells

For cell movement experiments, pairs of PCs, ISCs, and ISC-PC pairs were identified in microwell images at t=0. Distance between each cell in a pair was measured at t=0 and t=24. Relative change in distance (d^{Δ}) was calculated by subtracting distance at t=24 (d^{24}) from distance at t=0 (d^{0}) and normalizing to d^{0} (Supplementary Fig. S5A). Pairs of cells were only included in the experiment if they were alive at t=24hr, based on presence of EGFP or DSRED fluorescence. Distances were measured from the center of each cell to account for changes in cell size. Statistics were analyzed in Prism 6 (GraphPad, La Jolla, CA)by one-way ANOVA with Tukey's multiple comparisons test. To control for measurement error, primary intestinal epithelial cells were isolated and fixed in 4% PFA for 30min at room temperature, rinsed three times in PBS, and plated in MRA. Distance between fixed cell pairs (n=50) was calculated as per live cells, above. Results from the fixed cell experiment were compared to each group of live cell pairs by unpaired student's t-test to determine statistically significant movement.

Single cell isolation and qPCR

For single Paneth cell gene expression analysis, Paneth cells were sorted as described earlier and applied to a 10-17μm C1 Autoprep microfluidics chip (Fluidigm, San Francisco, CA) to generate a targeted cDNA library. Specific targets were pre-amplified using the following Taqman (Life Technologies) probe sets against genes of interest (supplemental material, Table S2). All other operations were conducted according to manufactures protocols. The specific target amplified (STA) libraries were applied to the Biomark HD microfluidics chip (Fluidigm) to conduct qPCR. The same probes sets used for the STA were used in the Biomark HD to detect relative gene expression levels. Binary gene expression (on/off) was calculated by differentially summing the number of cells with a positive Ct value or negative Ct value. The ratio of expressing vs. non-expressing cells was calculated by using 96 single

cells as the denominator for all genes assessed. Data were analyzed and heat maps were generated using the Fluidigm Real-Time PCR analysis software and delta-Ct values were calculated using the *Gapdh* or *18s* Ct for normalization.

Reproducibility of experiments

Figure 1F-1M shows representative data from MRA culture experiments, which have been independently replicated at least 70 times at the time of publication, and are ongoing in our lab.

Figure 3A shows representative data from 96 independent PC captures.

Figures 4A and 4F are from ISC-PC co-culture experiments and are representative of the 4,816 and 5,672 wells analyzed in each experiment, respectively.

Figure 5A shows representative data from 905 pairs of non-touching cells quantified in subsequent panels of the same figure.

Figure 6A shows representative images of retrieved rafts/enteroids from 192 total rafts.

Figure 6D shows representative morphology of cystic and columnar enteroids, from a total of 35 and 32 examined, respectively.

Supplementary Figure 2C-D shows representative tile scans of glass mounted MRAs, which have independently replicated at least 70 times at the time of publication, and are ongoing in our lab.

Supplementary Figure 5D-E shows representative retrieval and lysis of MRA rafts, which was conducted 259 times in the current manuscript and is ongoing in our lab.

Supplementary Material

Refer to Web version on PubMed Central for supplementary material.

Acknowledgments

The authors thank the UNC flow cytometry facility (P30CA06086), especially Barry Udis and Nancy Fisher. Casey Daniel Collins for help with quantification of survival. Dwight DeBree for data verification. Asad Ahmad and Pavak Shah for useful discussions regarding array fabrication and analysis. Danny Trotier for technical assistance with enteroid retrieval and graphics support. Drs. P. Kay Lund, Susan Henning (SJH), and Christopher Dekaney for useful discussions and critical review of the manuscript. ADG received partial salary support from U01 DK085541 (SJH).

Funding: This work was funded by the National Institutes of Health, R01 DK091427 (Magness), R03 EB013803 (Y. Wang/Magness), R01 EB012549 (Allbritton), Small Business Innovation Research R43 GM106421 (Magness/Y. Wang), U01 DK085507-01 (Li), University Cancer Research Fund of the University of North Carolina (Magness/Allbritton), and the Center for Gastrointestinal Biology and Disease P30 DK034987 (Magness, Y. Wang, Galanko). LL is a member of the Intestinal Stem Cell Consortium, supported by NIDDK and NIAID. ADG was supported by a UNC Graduate School Dissertation Completion Fellowship.

References

1. Sato T, Clevers H. Growing self-organizing mini-guts from a single intestinal stem cell: mechanism and applications. Science. 2013; 340:1190–1194. [PubMed: 23744940]
2. Barker N, et al. Identification of stem cells in small intestine and colon by marker gene Lgr5. Nature. 2007; 449:1003–1007. [PubMed: 17934449]
3. Gracz AD, Ramalingam S, Magness ST. Sox9-Expression Marks a Subset of CD24-expressing Small Intestine Epithelial Stem Cells that Form Organoids in vitro. Am J Physiol Gastrointest Liver Physiol. 2010
4. Sato T, et al. Single Lgr5 stem cells build crypt-villus structures in vitro without a mesenchymal niche. Nature. 2009; 459:262–265. [PubMed: 19329995]
5. Farin HF, Van Es JH, Clevers H. Redundant Sources of Wnt Regulate Intestinal Stem Cells and Promote Formation of Paneth Cells. Gastroenterology. 2012
6. Sato T, et al. Paneth cells constitute the niche for Lgr5 stem cells in intestinal crypts. Nature. 2011; 469:415–418. [PubMed: 21113151]
7. Formeister EJ, et al. Distinct SOX9 levels differentially mark stem/progenitor populations and enteroendocrine cells of the small intestine epithelium. American journal of physiology Gastrointestinal and liver physiology. 2009; 296:G1108–1118. [PubMed: 19228882]
8. Snippert HJ, et al. Intestinal crypt homeostasis results from neutral competition between symmetrically dividing Lgr5 stem cells. Cell. 2010; 143:134–144. [PubMed: 20887898]
9. Shackleton M, et al. Generation of a functional mammary gland from a single stem cell. Nature. 2006; 439:84–88. [PubMed: 16397499]
10. Till JE, Mc CE. A direct measurement of the radiation sensitivity of normal mouse bone marrow cells. Radiat Res. 1961; 14:213–222. [PubMed: 13776896]
11. Lecault V, et al. High-throughput analysis of single hematopoietic stem cell proliferation in microfluidic cell culture arrays. Nat Methods. 2011; 8:581–586. [PubMed: 21602799]
12. Wang Y, et al. Micromolded arrays for separation of adherent cells. Lab Chip. 2010; 10:2917–2924. [PubMed: 20838672]
13. Vintersten K, et al. Mouse in red: red fluorescent protein expression in mouse ES cells, embryos, and adult animals. Genesis. 2004; 40:241–246. [PubMed: 15593332]
14. Wang F, et al. Isolation and characterization of intestinal stem cells based on surface marker combinations and colony-formation assay. Gastroenterology. 2013; 145:383–395 e381-321. [PubMed: 23644405]
15. Carpenter AE, et al. CellProfiler: image analysis software for identifying and quantifying cell phenotypes. Genome Biol. 2006; 7:R100. [PubMed: 17076895]
16. Powell AE, et al. The pan-ErbB negative regulator Lrig1 is an intestinal stem cell marker that functions as a tumor suppressor. Cell. 2012; 149:146–158. [PubMed: 22464327]
17. Gracz AD, et al. CD24 and CD44 Mark Human Intestinal Epithelial Cell Populations with Characteristics of Active and Facultative Stem Cells. Stem Cells. 2013
18. von Furstenberg RJ, et al. Sorting mouse jejunal epithelial cells with CD24 yields a population with characteristics of intestinal stem cells. Am J Physiol Gastrointest Liver Physiol. 2010
19. Buczacki SJ, et al. Intestinal label-retaining cells are secretory precursors expressing Lgr5. Nature. 2013; 495:65–69. [PubMed: 23446353]
20. Schwitalla S, et al. Intestinal tumorigenesis initiated by dedifferentiation and acquisition of stem-cell-like properties. Cell. 2013; 152:25–38. [PubMed: 23273993]
21. van Es JH, et al. Dll1(+) secretory progenitor cells revert to stem cells upon crypt damage. Nat Cell Biol. 2012
22. Shah PK, Hughes MR, Wang Y, Sims CE, Allbritton NL. Scalable synthesis of a biocompatible, transparent and superparamagnetic photoresist for microdevice fabrication. J Micromech Microeng. 2013; 23
23. Montgomery RK, et al. Mouse telomerase reverse transcriptase (mTert) expression marks slowly cycling intestinal stem cells. Proc Natl Acad Sci U S A. 2011; 108:179–184. [PubMed: 21173232]

24. Munoz J, et al. The Lgr5 intestinal stem cell signature: robust expression of proposed quiescent '+4' cell markers. The EMBO journal. 2012; 31:3079–3091. [PubMed: 22692129]
25. Takeda N, et al. Interconversion between intestinal stem cell populations in distinct niches. Science. 2011; 334:1420–1424. [PubMed: 22075725]
26. Yan KS, et al. The intestinal stem cell markers Bmi1 and Lgr5 identify two functionally distinct populations. Proc Natl Acad Sci U S A. 2012; 109:466–471. [PubMed: 22190486]
27. Kim TH, et al. Broadly permissive intestinal chromatin underlies lateral inhibition and cell plasticity. Nature. 2014
28. Stamataki D, et al. Delta1 expression, cell cycle exit, and commitment to a specific secretory fate coincide within a few hours in the mouse intestinal stem cell system. PLoS One. 2011; 6:e24484. [PubMed: 21915337]
29. Jensen J, et al. Control of endodermal endocrine development by Hes-1. Nat Genet. 2000; 24:36–44. [PubMed: 10615124]
30. Yang Q, Bermingham NA, Finegold MJ, Zoghbi HY. Requirement of Math1 for secretory cell lineage commitment in the mouse intestine. Science. 2001; 294:2155–2158. [PubMed: 11739954]
31. Kanatsu-Shinohara M, et al. Reconstitution of mouse spermatogonial stem cell niches in culture. Cell Stem Cell. 2012; 11:567–578. [PubMed: 23040482]
32. Wu AR, et al. Quantitative assessment of single-cell RNA-sequencing methods. Nat Methods. 2014; 11:41–46. [PubMed: 24141493]
33. Gobaa S, et al. Artificial niche microarrays for probing single stem cell fate in high throughput. Nat Methods. 2011; 8:949–955. [PubMed: 21983923]
34. Roccio M, Gobaa S, Lutolf MP. High-throughput clonal analysis of neural stem cells in microarrayed artificial niches. Integr Biol (Camb). 2012; 4:391–400. [PubMed: 22307554]
35. Burdick JA, Watt FM. High-throughput stem-cell niches. Nat Methods. 2011; 8:915–916. [PubMed: 22036745]
36. Eiraku M, et al. Self-organizing optic-cup morphogenesis in three-dimensional culture. Nature. 2011; 472:51–56. [PubMed: 21475194]
37. Lancaster MA, et al. Cerebral organoids model human brain development and microcephaly. Nature. 2013; 501:373–379. [PubMed: 23995685]
38. Sato T, et al. Long-term expansion of epithelial organoids from human colon, adenoma, adenocarcinoma, and Barrett's epithelium. Gastroenterology. 2011; 141:1762–1772. [PubMed: 21889923]
39. Gong S, et al. A gene expression atlas of the central nervous system based on bacterial artificial chromosomes. Nature. 2003; 425:917–925. [PubMed: 14586460]
40. Barker N, et al. Identification of stem cells in small intestine and colon by marker gene Lgr5. Nature. 2007; 449:1003–1007. [PubMed: 17934449]
41. Wang F, et al. Isolation and characterization of intestinal stem cells based on surface marker combinations and colony-formation assay. Gastroenterology. 2013; 145:383–395 e381-321. [PubMed: 23644405]
42. Sato T, et al. Paneth cells constitute the niche for Lgr5 stem cells in intestinal crypts. Nature. 2011; 469:415–418. [PubMed: 21113151]
43. Sato T, et al. Single Lgr5 stem cells build crypt-villus structures in vitro without a mesenchymal niche. Nature. 2009; 459:262–265. [PubMed: 19329995]
44. Schindelin J, et al. Fiji: an open-source platform for biological-image analysis. Nat Methods. 2012; 9:676–682. [PubMed: 22743772]
45. Pai JH, et al. Photoresist with low fluorescence for bioanalytical applications. Anal Chem. 2007; 79:8774–8780. [PubMed: 17949059]
46. Wang Y, et al. Micromolded arrays for separation of adherent cells. Lab Chip. 2010; 10:2917–2924. [PubMed: 20838672]
47. Jackman RJ, Duffy DC, Ostuni E, Willmore ND, Whitesides GM. Fabricating large arrays of microwells with arbitrary dimensions and filling them using discontinuous dewetting. Anal Chem. 1998; 70:2280–2287. [PubMed: 21644640]

48. Gracz AD, Puthoff BJ, Magness ST. Identification, isolation, and culture of intestinal epithelial stem cells from murine intestine. Methods in molecular biology. 2012; 879:89–107. [PubMed: 22610555]

49. Gracz AD, Ramalingam S, Magness ST. Sox9-Expression Marks a Subset of CD24-expressing Small Intestine Epithelial Stem Cells that Form Organoids in vitro. Am J Physiol Gastrointest Liver Physiol. 2010

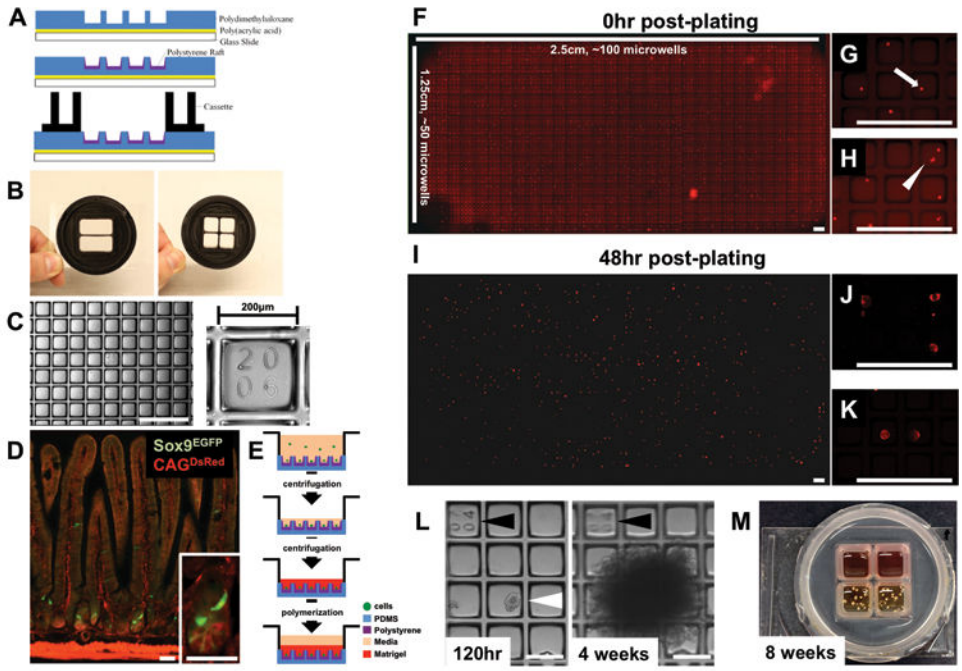

Figure 1. Modified MRAs are compatible with long-term culture of primary ISCs

(**A**) Completed MRAs consist of polystyrene "raft"-lined PDMS microwells mounted to a glass slide with a thin layer of PAA, and attached to a cassette containing media chambers. (**B**) Cassettes can be scaled to divide a single MRA into 2 or 4 separate media reservoirs. (**C**) Microwells are 200μm^2, arranged in a grid, and the physical addresses stamped into PDMS at 5 well intervals. Scale bar represents 600μm (**D**) ISCs are isolated from *Sox9*^{EGFP}:*CAGDsRed* transgenic mice, which express dsRed throughout the intestinal epithelium. Scale bars represent 50μm. (**E**) Isolated cells are seeded into microwells through centrifugation in media, and then overlaid with Matrigel. (**F**) ISCs are randomly distributed across arrays immediately after plating, with some microwells containing single ISCs (**G**, arrow), and others containing multiple ISCs (**H**, arrowhead). (**I**) Imaging of the same array at 48hrs reveals widespread enteroid formation, with (**J**,**K**) typical cystic growth of early structures. Scale bars for panels F-K represent 600μm. (**L**) Long-term culture experiments demonstrate that developed ISCs grow out from their original microwells over the course of 4 weeks, and (**M**) can be sustained in the array format for 8 weeks or longer (upper two wells are empty in this image). Scale bars represent 200μm.

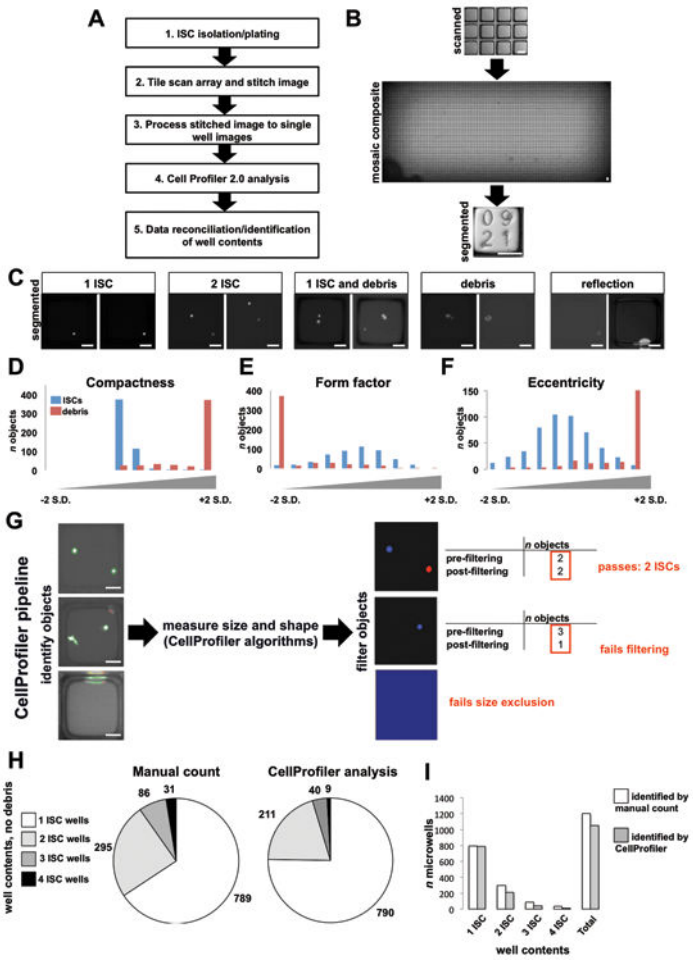

Figure 2. Software-assisted post-hoc analysis identifies initial well contents of MRA culture

(**A**) A defined workflow facilitates post-hoc image analysis to identify well contents in MRA cultures. (**B**) Tile-scanned images are stitched together to form a single composite image, which is then segmented into individual microwell images, each with a unique address corresponding to its physical position in the array. Scale bars represent 100μm. (**C**) Visual examination of individual microwells reveals the presence of debris and fluorescent glare as well as ISCs. Scale bars represent 50μm. (**D-F**) To distinguish between true ISCs and debris/noise, visually scored wells were analyzed by CellProfiler to determine the distribution profiles of target events (ISC, blue) and debris (red) for the variables compactness, form factor, and eccentricity. (**G**) A novel CellProfiler pipeline that identifies objects and applies filters based on the size and shape profiles of known ISCs is used to analyze segmented microwell images. If the number of objects initially identified by CellProfiler is equal to those that pass filtering parameters, the microwell passes inclusion criteria (**G**, top microwell), otherwise it is excluded as debris containing or empty (**G**, middle and bottom microwells). Scale bars represent 50μm. (**H & I**) Application of the optimized pipeline to randomly selected microwell images reveals an overall accuracy of 99.87%, 71.53%, 46.51%, and 29.03% for wells containing 1, 2, 3, and 4 ISCs, respectively (n = 2,254 randomly selected microwells).

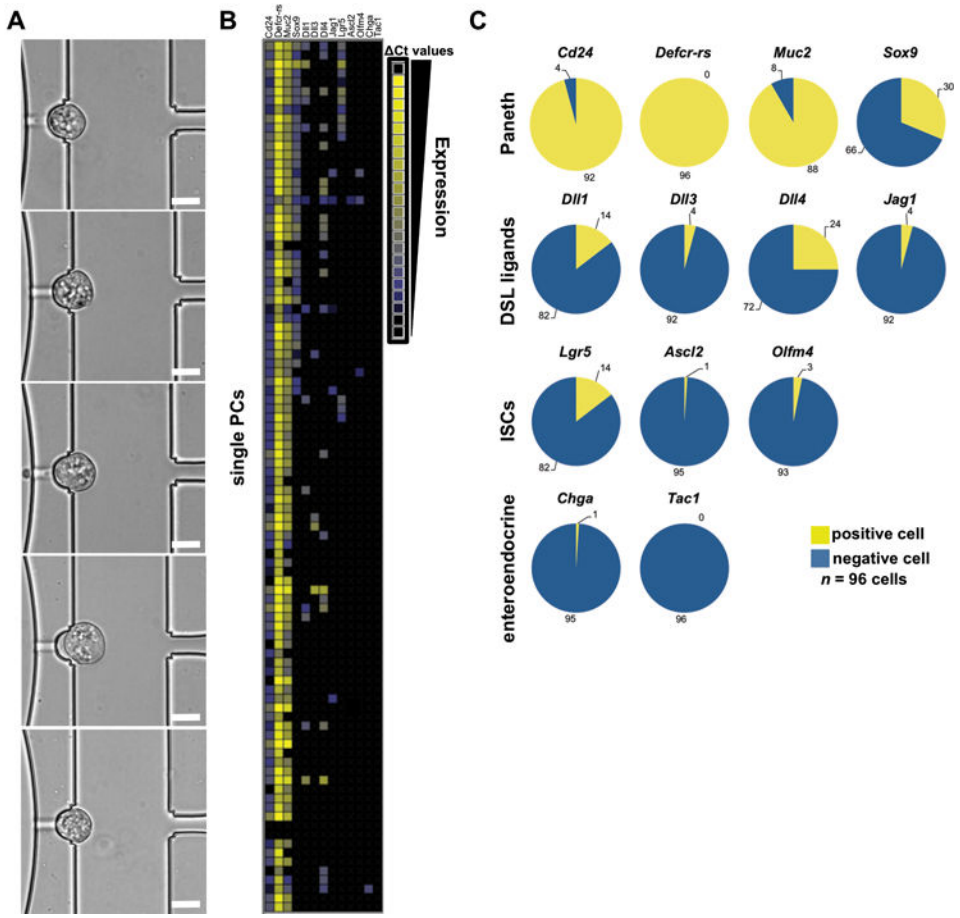

Figure 3. Single cell qPCR confirms Paneth cell purity

To assess non-PC contamination in CD24^{high}:SSC^{high}:*Sox9EGFP*^{neg} populations at the single cell level, we isolated, lysed, and processed 96 individual PCs for cDNA using the Fluidigm C1 microfluidics-based platform. (**A**) Single cells "captured" on the microfluidics chip contained granules and were morphologically consistent with PCs prior to cell lysis. Scale bars represent 10μm. (**B**) Gene expression analyses indicate that single cells are enriched for PC markers and do not express ISC or enteroendocrine markers. (**C**) All cells expressed the PC specific transcript, *Defcr-rs*. Additionally, isolated cells variably express DSL ligands associated with ISC niche function (n = 96 PCs).

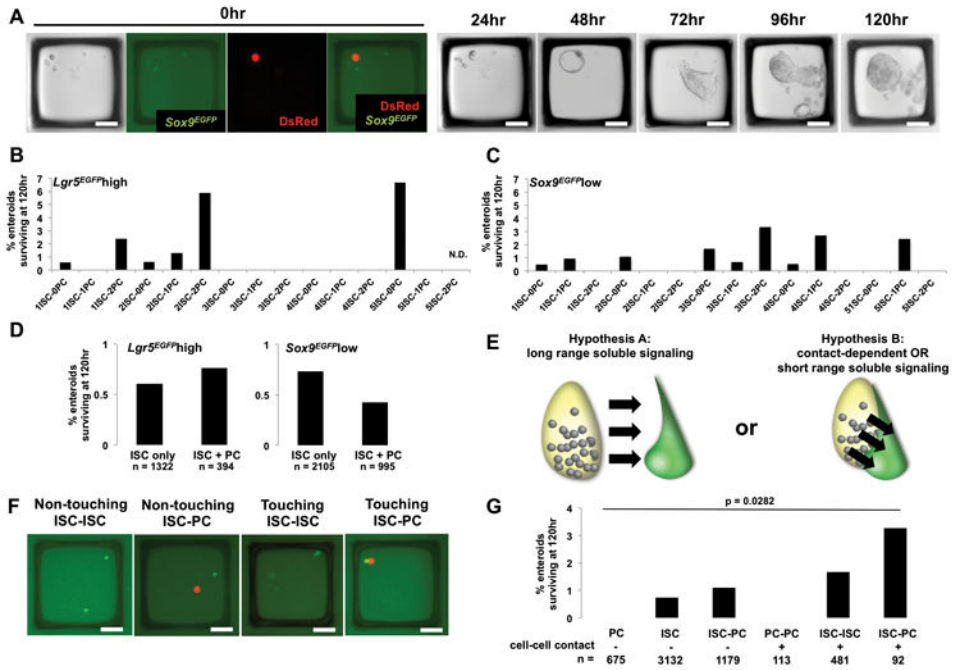

Figure 4. Cell-to-cell contact is required for Paneth cell influenced survival of ISCs *in vitro*

(**A**) PCs are isolated from *Sox9*^{EGFP}:*CAGDsRed* mice and co-cultured with ISCs from *Sox9*^{EGFP} or *Lgr5*^{EGFP} mice lacking the constitutive *DsRed* transgene, allowing for independent tracking of ISC and PC growth in MRAs. (**B,C**) Quantification of enteroid formation across 15 combinations of ISCs and PCs in experiments using ISCs isolated based on *Sox9* and *Lgr5* biomarker expression demonstrates no significant increase in enteroid formation at 120hr associated with any one condition. Additionally, we were unable to identify any clear trends between PC number and enteroid development by ISCs (conditional logistic regression, n = 4,816 microwells, replicates per group listed in Supplementary Table 1). (**D**) Analysis of overall enteroid formation by ISCs only and ISC-PC co-cultures, regardless of cell number per microwell, also fails to produce a significant effect associated with PC presence (conditional logistic regression, n = 4,816 microwells). (**E**) Because all data were analyzed *post-hoc* from existing images, we were able to test the alternative hypothesis that cell-cell contact is required for PCs to have a niche effect *in vitro*. (**F,G**) Interestingly, when we grouped initial well contents by whether or not ISCs were in contact with other ISCs or PCs at t = 0, we found that ISC-PCs in direct contact were more likely to form enteroids than ISCs alone (conditional logistic regression, p = 0.0282, n = 5,672 microwells). Single PCs and PC-PC doublets did not form enteroids and were excluded from statistical analysis. Data is derived from experiments conducted in replicate for each ISC biomarker. Cell-to-cell contact data is pooled from 8 independent MRAs from 4 *Sox9*^{EGFP} and *Lgr5*^{EGFP} animals. N.D. = no data; no microwells had initial contents matching this combination. All scale bars represent 50μm.

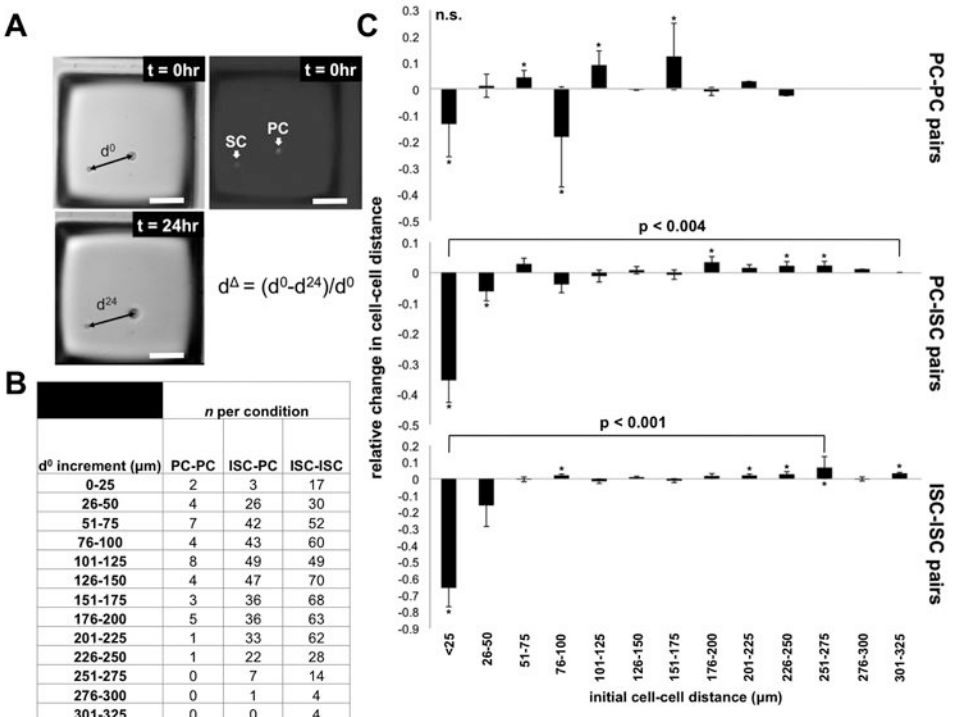

d⁰ increment (μm)	PC-PC	ISC-PC	ISC-ISC
0-25	2	3	17
26-50	4	26	30
51-75	7	42	52
76-100	4	43	60
101-125	8	49	49
126-150	4	47	70
151-175	3	36	68
176-200	5	36	63
201-225	1	33	62
226-250	1	22	28
251-275	0	7	14
276-300	0	1	4
301-325	0	0	4
total	39	345	521

Figure 5. Single cells do not form cell-cell contacts in microwells after initial plating

(A) Initial ("d^0") and 24hr ("d^{24}") distances were measured from the centers of non-touching cells to determine positive or negative changes in distance, normalized to the initial distance ("d^Δ"). To examine the possibility that cell-cell signaling might be affecting relative cell movement, pairs were grouped and compared in 25μm d^0 increments. **(B)** Number of non-touching pairs examined per distance. **(C)** Non-touching pairs of cells with a d^0 value ≤25μm demonstrate statistically significant movement away from one another, relative to d^Δ associated with pairs having a d^0 value ≥25μm. d^Δ was calculated for pairs of fixed cells (n = 50) and compared to live cell movement to control for non-specific changes in distance. Scale bars represent 50μm. Asterisks represent statistically significant movement, relative to fixed cells (unpaired t-test, $p < 0.05$. Exact p values presented in Supplementary Table 3).

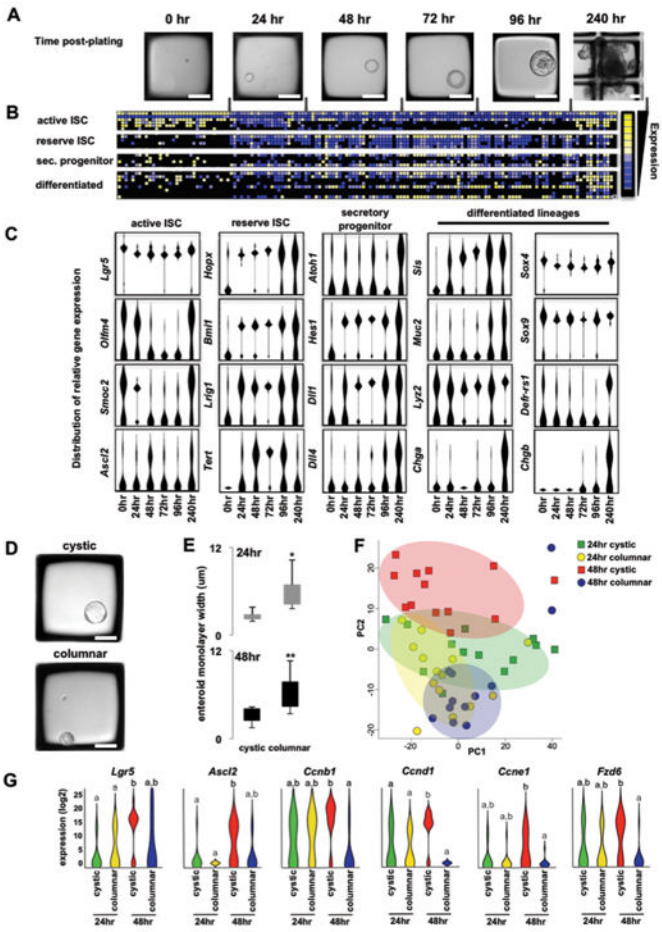

Figure 6. Microraft retrieval facilitates gene expression analysis of enteroid development and morphology

(**A**) *Lgr5*^{high} cells were seeded in MRAs containing magnetic polystyrene rafts. Individual rafts with either single cells or developing enteroids were collected every 24-hours for 4 days and again at day 10 (240 hrs) post-plating. High-throughput qPCR was used to interrogate gene expression from the contents in each raft. (**B**) A heat map of dCT values demonstrates high levels of active ISC biomarkers at t=0. Later time points demonstrate an increase in secretory progenitor markers followed by differentiated cell markers consistent with a progression toward fully mature enteroids at 240 hours post-plating. (**C**) Violin plots of CT values show distribution of gene expression levels during each day of enteroid development. (**D**) Early enteroids adopt a cystic or columnar morphology; 48hr shown here. **(E)** Quantification of cell width in enteroid monolayers validates the morphological difference between cystic and columnar enteroids (n = 20 cystic and 17 columnar enteroids at 24hr; 15 cystic and 15 columnar at 48hr. unpaired t-test; * = p = 8.1 x 10^{-9}; ** = p = 0.0003). **(F)** PCA demonstrates that cystic and columnar enteroids become increasingly genotypically distinct at 48hr. **(G)** Cystic enteroids express significantly higher levels of cyclins *Ccnb1*, *Ccnd1*, and *Ccne1*, as well as higher levels of *Lgr5*, *Ascl2*, and Wnt receptor *Fzd6*, suggesting that cystic morphology is associated with active proliferation (n = 13 cystic and 14 columnar enteroids at 24hr; 13 cystic and 12 columnar at 48hr; different letters

represent statistical significance; one-way ANOVA, $p < 0.05$. Exact p values presented in Supplementary Table 3). All scale bars represent 50μm.

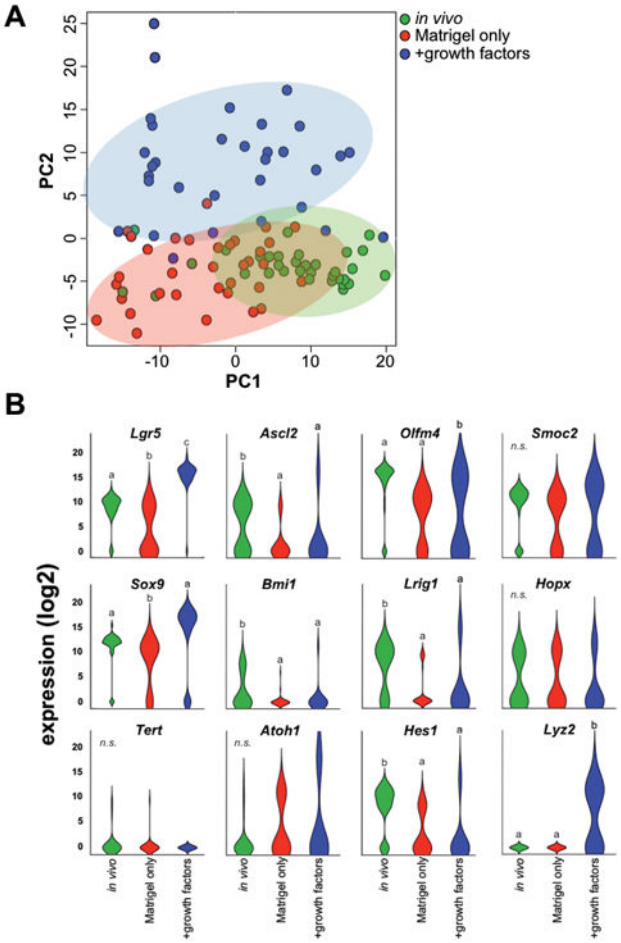

Figure 7. Culture conditions drive transcriptional changes in single *Lgr5*^{high} cells

Single *Lgr5*^{high} ISCs were sorted directly into lysis buffer, or plated in MRAs with and without growth factors (EGF, Noggin, Jagged-1, CHIR99021, LY2157299, and Thiazovivin) for 2hrs. **(A)** Single *Lgr5*^{high} cells clustered according to their treatment group by PCA. **(B)** Exposure to growth factors resulted in a significant upregulation of *Lgr5* as well as a significant downregulation of *Bmi1* and *Lrig*. No significant changes were detected for *Hopx* or *Tert*, regardless of treatment, suggesting that co-expression of *Lgr5* with these markers is variable at the single cell level, both *in vivo* and in very early Matrigel cultures. Interestingly, despite elevated expression of *Lgr5* in the presence of growth factors, these conditions also elicited a downregulation of *Olfm4* in a subpopulation of single ISCs. We also noted that elevated *Lyz2* expression was driven by growth factor conditions, and may indicate an early culture-dependent divergence from ISC-associated transcriptional programs in a subset of *Lgr5*^{high} cells (n = 36 cells per condition, different letters represent statistical significance; one-way ANOVA, $p < 0.05$. Exact p values presented in Supplementary Table 3).